Irreversibility of Marine Climate Change Impacts under Carbon Dioxide Removal

Xinru Li[1], Kirsten Zickfeld[1], Sabine Mathesius[1], Karen Kohfeld[2], and J. B. Robin Matthews[3]

[1] Department of Geography, Simon Fraser University, Burnaby, B.C., Canada[1]

[2] School of Resource & Environmental Management, Simon Fraser University, Burnaby, B.C., Canada

[3] Université Paris-Saclay, Saint-Aubin, France

Corresponding author: Xinru Li (xinru.li@alumni.ubc.ca)

Key Points:

- Changes in sea surface temperature, pH and dissolved oxygen concentration in overshoot scenarios are largely reversible.
- Changes in average ocean values of these variables are not reversible centuries after the overshoot is removed.
- Spatial changes in these variables exhibit substantial differences between overshoot and non-overshoot scenarios in some regions.

[1] Xinru Li is now in the Department of Geography, University of British Columbia, Vancouver, B.C., Canada.

Abstract

Artificial carbon dioxide removal (CDR) from the atmosphere has been proposed as a measure for mitigating climate change and restoring the climate system to a target state after exceedance ("overshoot"). This research investigates to what extent overshoot and subsequent recovery of a given cumulative CO_2 emissions level by CDR leaves a legacy in the marine environment using an Earth system model. We use RCP2.6 and its extension to year 2300 as the reference scenario and design a set of cumulative emissions and temperature overshoot scenarios based on other RCPs. Our results suggest that the overshoot and subsequent return to a reference cumulative emissions level would leave substantial impacts on the marine environment. Although the changes in sea surface temperature, pH and dissolved oxygen are largely reversible, global mean values and spatial patterns of these variables differ significantly from those in the reference scenario when the reference cumulative emissions are attained.

Plain Language Summary

Commitments by countries to reduce emissions of carbon dioxide (CO_2) fall short of what is needed to limit global warming to below 2°C, a goal of the Paris Agreement, creating a risk that the 2°C limit may be exceeded. Restoring global temperature to a target level after exceedance ("overshoot") requires artificial carbon dioxide removal (CDR) from the atmosphere. Earlier studies showed that changes in surface air temperature can be reversed by CDR, but climate variables that take longer to respond to changes in atmospheric CO_2 are slower to reverse. In this research we investigate to what extent the impacts of overshoot on the marine environment can be reversed with CDR. We show that the ocean responds slowly to a decrease in atmospheric CO_2 concentration by CDR, particularly for scenarios with large levels of overshoot. The overshoot results in substantial impacts on the marine environment for centuries with potentially detrimental effects for marine ecosystems.

1 Introduction

In 2015 the Paris Climate Change Conference adopted the Paris Agreement that calls for "holding the increase in the global average temperature to well below 2°C above pre-industrial levels" (UNFCCC, 2015). Countries' current pledges for CO_2 emissions reductions are inconsistent with this goal (Rogelj et al., 2016; UNFCCC, 2016). Thus, unless greenhouse gas emissions decrease rapidly, limiting warming to well below 2°C without temporarily exceeding that level is unlikely.

CO_2, the principal anthropogenic greenhouse gas, has a long atmospheric lifetime as its concentration remains elevated for centuries to millennia following cessation of anthropogenic emissions (Eby et al., 2009; Solomon et al., 2009). Several studies showed that the reduction of CO_2 emissions to net zero can stabilize global warming, but not reverse it (Matthews & Caldeira, 2008; Lowe et al., 2009; Frölicher & Joos, 2010; Gillett et al., 2011; Zickfeld et al., 2013; Ehlert & Zickfeld, 2017). Global mean temperature can be restored to a target level on geological (>10,000 years) timescales, implying that global warming is irreversible on human timescales (decades to a century) (Eby et al., 2009; Solomon et al., 2009). Thus, carbon dioxide removal (CDR) from the atmosphere, also referred to as "negative CO_2 emissions", has been proposed for mitigating CO_2-induced climate changes and restoring the climate system to a state that avoids "dangerous" impacts (UNFCCC Article 2, 1992), if climate actions fail to reduce emissions sufficiently fast to comply with the "well below 2°C" climate limit.

Previous studies indicated that changes in surface air temperature due to anthropogenic CO_2 emissions can be reversed through net-negative CO_2 emissions (Cao & Caldeira, 2010; MacDougall, 2013; Jones et al., 2016;Tokarska & Zickfeld, 2015), while climate variables with long response timescales, for example ocean thermal expansion, exhibit a delay in their responses to net-negative CO_2 emissions (Boucher et al., 2012; Bouttes et al., 2013b; MacDougall, 2013; Mathesius et al., 2015; Tokarska & Zickfeld, 2015; Ehlert & Zickfeld, 2018). Mathesius et al. (2015) showed that delayed emissions reduction followed by implementation of negative emissions at a likely unfeasible rate cannot entirely restore global mean ocean temperature, dissolved oxygen and pH to their levels in a low-emission scenario. The lagged behavior in ocean conditions implies that CDR could be ineffective at reversing climate change impacts on the ocean, due to the ocean's long (millennial) response timescale.

This research aims to further investigate the reversibility of changes in ocean conditions after the implementation of net-negative CO_2 emissions using an Earth System model of intermediate complexity. We place the analysis in the context of emission scenarios that temporarily exceed 2°C global warming relative to pre-industrial conditions and later stabilize warming below 2°C. We compare the ocean response in such "overshoot" scenarios to that in a reference scenario that limits warming to below 2°C with limited overshoot when the same amount of cumulative CO_2 emissions is reached. We examine the change in ocean conditions under different levels of surface air temperature and cumulative CO_2 emissions overshoot and subsequent return to the levels in a reference low-emission scenario.

2 Model and Simulations

This study employs the University of Victoria Earth System Climate Model (UVic ESCM), an Earth System Model of Intermediate Complexity (EMIC). This model consists of an energy moisture balance model of the atmosphere with dynamical wind feedback coupled to a three-dimensional ocean general circulation model and a dynamic/thermodynamic sea ice model (Weaver et al., 2001). The physical climate model is coupled to a land surface model, a dynamic terrestrial vegetation model, ocean inorganic and organic carbon cycle models and a sediment model (Eby et al., 2009) (see Text S1 for further details).

To force the model a set of future CO_2 emission scenarios (Figure 1a) is designed based on the Representative Concentration Pathways (RCPs) and their extensions (EXPs) until year 2300 (Meinshausen et al., 2011). We devise a "reference" scenario that follows RCP2.6 and its extension until year 2300, which is consistent with limiting global mean temperature increase to 2°C above pre-industrial levels in 80% of CMIP5 models (Collins et al., 2013). A set of "overshoot" scenarios is designed based on the other RCPs (RCP4.5, RCP6 and RCP8.5), which are modified in such a way that their cumulative CO_2 emissions temporarily exceed and then converge to those of RCP/EXP2.6 in 2300 (Figures 1a and S1; see Text S2 for further details). Land use change-related CO_2 emissions are prescribed to follow RCP2.6 and are the same for all scenarios.

The overshoot scenarios are named according to the maximum net-negative CO_2 emissions rate applied in each overshoot scenario: 5 GtC/yr, 9 GtC/yr and 15 GtC/yr in RCP4.5-CDR5, RCP6-CDR9 and RCP8.5-CDR15 respectively. Though negative emissions of 15 GtC/yr are at the upper end of the range considered feasible (The National Academies Press, 2019), this rate is used here to explore the implications of a large range of cumulative emissions overshoot. Negative CO_2 emissions are applied to the model without specifying any particular CDR

technology. The removed CO_2 is assumed to be taken out of the ocean-atmosphere system permanently (e.g., by storage underground).

The model was spun up for 10,000 years under year-850 conditions, following the protocol for the EMIC model intercomparison project conducted in support of the Fifth Assessment Report of IPCC (Eby, 2013). The long model spin-up practically eliminated any drift. The model was then initialized from year-850 equilibrium state and forced with observed atmospheric CO_2 concentration, radiative forcing from non-CO_2 greenhouse gases, sulphate aerosols, land-use changes, and natural forcings (orbital, solar and volcanic) to the year 2006. This historical simulation provided the initial condition for a range of future simulations (2006-3000) forced with the CO_2 emission scenarios described above. In addition to CO_2 emissions, radiative forcing from non-CO_2 greenhouse gases was prescribed to follow RCP2.6 and its extension to 2300 and was held fixed at year-2300 levels thereafter. Aerosol radiative forcing (direct effect) and land cover change followed RCP2.6 until 2100 and were held constant thereafter. Natural forcings were specified as follows: orbital forcing was held fixed at year-2005 levels; solar irradiance was set to repeat the last solar cycle (1996-2008); and volcanic forcing was set to zero. Non-CO_2 forcings are the same in all scenarios.

3 Results

3.1 Global Average Response

We analyze differences in climate variables between the reference scenario RCP2.6 and the overshoot scenarios, with a focus on year 2300 when the same cumulative CO_2 emissions are achieved in all scenarios (Figure S1). The atmospheric CO_2 concentration in all scenarios increases with net positive anthropogenic CO_2 emissions and starts to decline when CO_2 uptake by natural carbon sinks exceeds net CO_2 emissions. The CO_2 concentration in the overshoot scenarios is reduced to a level lower than that in RCP2.6 by 20 ppmv (RCP4.5-CDR5) to 53 ppmv (RCP8.5-CDR15) in 2300 (Figure 1b). This considerable difference in atmospheric CO_2 concentration between RCP2.6 and the overshoot scenarios is due to inertia in the ocean carbon cycle response (Figure S2), which lags the decline in atmospheric CO_2. The initial rise in atmospheric CO_2 causes surface air temperature (SAT) to increase. Implementation of net-negative emissions leads to a decline in SAT in the overshoot scenarios, with SAT being warmer than in RCP2.6 by 0.1°C (RCP4.5-CDR5) to 0.3°C (RCP8.5-CDR15) in 2300 (Figure 1c). This result indicates that emission pathways with larger overshoot result in slightly different SAT despite the same amount of cumulative CO_2 emissions.

Globally averaged sea surface temperature (SST) increases with the rising CO_2 concentration and starts to decline 15 years (RCP8.5-CDR15) to 50 years (RCP4.5-CDR5) after the decline in atmospheric CO_2. In 2300, SST in the overshoot scenarios exceeds that in RCP2.6 by 0.1°C (RCP4.5-CDR5) to 0.3°C (RCP8.5-CDR15) (Figure 1d). Global average ocean temperature (OT) increases during the whole simulation in RCP2.6 (Figure 1h). In the overshoot scenarios, OT peaks and declines following implementation of net negative emissions, and then increases again. The decline of OT lags the reduction in atmospheric CO_2 concentration by about 120 years (RCP8.5-CDR15) to 180 years (RCP4.5-CDR5). OT in the overshoot scenarios is warmer than in RCP2.6 by 0.2°C (RCP4.5-CDR5) to 0.6°C (RCP8.5-CDR15) in 2300 (Figure 1h). Sea level rise due to ocean thermal expansion (i.e. thermosteric sea level rise) shows similar

lagged responses as OT, with larger thermosteric sea level rise in the overshoot scenarios relative to RCP2.6 by 12 cm (RCP4.5-CDR5) to 38 cm (RCP8.5-CDR15) in 2300 (Figure S3).

Changes in dissolved oxygen concentration (DO) are determined by changes in ocean temperature, which affect oxygen solubility in sea water, ocean ventilation and biological processes, which affect the production and consumption of DO. Sea surface DO declines with rising SST and recovers after implementation of net negative CO_2 emissions, reaching a level close to 2.0% below pre-industrial in 2300 in all scenarios (Figure 1e). Global average DO in RCP2.6 decreases over the whole simulation (Figure 1i). In the overshoot scenarios, global average ocean DO continues to decline for 120 years (RCP8.5-CDR15) to 190 years (RCP4.5-CDR5) after the peak in atmospheric CO_2 concentration, and then temporarily increases before declining again (Figure 1i). In 2300, the decrease in global average ocean DO ranges from 7.9 % (RCP4.5-CDR5) to 8.9 % (RCP8.5-CDR15) below preindustrial, compared to 6.7% in RCP2.6 (Figure 1i). After year 2300, global average ocean DO in the overshoot scenarios decreases again until the end of the simulation, with the DO decline rate varying between scenarios (Figure 1i). Interestingly, the rate of global average DO decline is lowest in the scenario with the largest overshoot (RCP8.5-CDR15) (Figure 1i), possibly caused by more vigorous ocean circulation (Figure S4, S5).

Sea surface pH drops with rising atmospheric CO_2 and recovers when the CO_2 concentration declines (Figure 1b, 1f). In 2300, the decrease in sea surface pH below preindustrial in the overshoot scenarios is smaller than that in RCP2.6 by 0.01 units (RCP4.5-CDR5) to 0.03 units (RCP8.5-CDR15) (Figure 1f), which reflects the lower atmospheric CO_2 concentration in the overshoot scenarios discussed previously. Global average ocean pH in RCP2.6 decreases slightly over the whole simulation (Figure 1g). In the overshoot scenarios, global average ocean pH reaches a minimum between years 2190 (RCP8.5-CDR15) and 2210 (RCP4.5-CDR5) and then recovers. In 2300, the decrease in global average ocean pH ranges from 0.10 units (RCP4.5-CDR5) to 0.12 units (RCP8.5-CDR15) below preindustrial, compared to 0.08 units in RCP2.6 (Figure 1g). The slower recovery of entire ocean pH compared to sea surface pH in 2300 can be attributed to slow upward mixing of excess CO_2 and enhanced ocean stratification, which further slows the release of CO_2 to the atmosphere and the reversal of pH decline in the ocean interior.

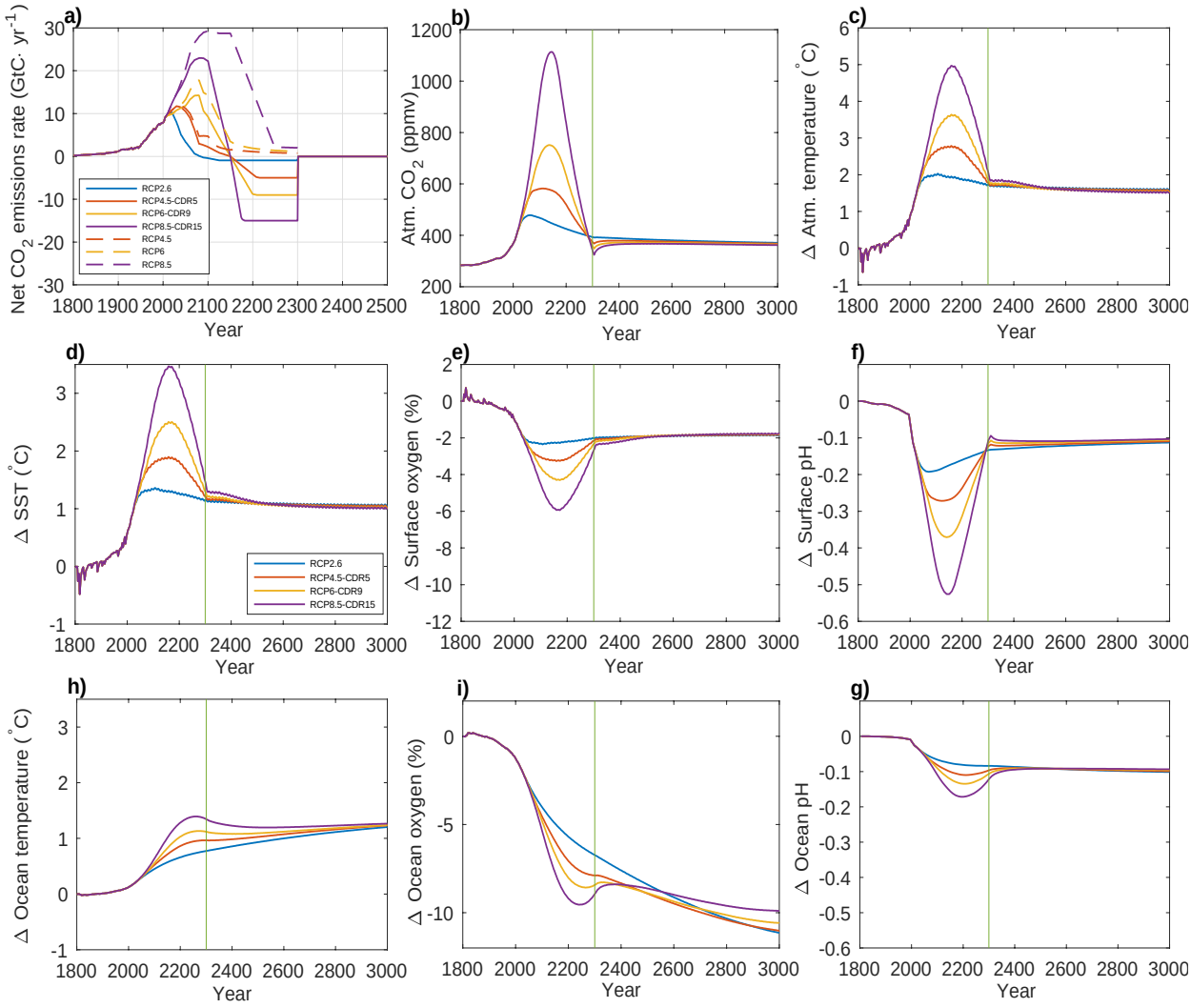

Figure 1. Time series of global mean variables for the reference (RCP2.6) and overshoot scenarios. **a,** net anthropogenic CO_2 emissions rate ($GtC \cdot yr^{-1}$) (defined as CO_2 emissions from fossil fuels and land-use change minus CO_2 removals). RCP scenarios are shown for comparison (dashed lines). **b,** atmospheric CO_2 concentration (ppmv). **c,** surface air temperature change (°C). **d,** sea surface temperature change (°C). **e,** sea surface dissolved oxygen concentration change (%). **f,** sea surface pH change (total pH scale). **h,** global average ocean temperature change (°C). **i,** global average ocean dissolved oxygen concentration change (%). **g,** global average ocean pH change. Changes in panels **c**-**g** are relative to year 1800. Note that panel **a** has a different horizontal scale than the other panels.

3.2 Regional Ocean Impacts

At the time the cumulative CO_2 emissions overshoot is removed (year 2300), the spatial distribution of sea surface variables (temperature, dissolved oxygen concentration and pH) exhibits large differences between the overshoot scenarios and the reference scenario RCP2.6, despite similar global mean sea surface values.

In year 2300, most sea surface areas are warmer relative to preindustrial except the North Atlantic south of Greenland and the Weddell Sea where SST is cooler (Figure S6a-d). Large sea surface areas are warmer in the overshoot scenarios than in RCP2.6 in 2300, particularly in the

Southern Ocean between 40°S and 60°S (Figure 2a-c). The larger warming in this region is associated with stronger Southern Hemisphere westerlies (driven by a stronger surface air temperature gradient between 30°S and 60°S; Figure S7), leading to a more vigorous meridional overturning circulation and enhanced subduction of surface waters around 60°S (Fyfe et al., 2007). In contrast, SST is cooler in the North Atlantic south of Greenland in 2300 relative to RCP2.6 (Figure 2a-c). The cooler SST is driven by a weakening of the Atlantic meridional overturning circulation (AMOC) (Figure S8), which results in reduced northward heat transport in the UVic Model (Saenko et al., 2004).

Large areas of the interior ocean are warmer relative to preindustrial in 2300 (Figure S6e-h), with larger warming in the overshoot scenarios than in RCP2.6, particularly at 200-2,000 m depth in the latitudinal band of 60°S to 60°N (Figure 2d-f). Heat enters the interior ocean in areas of North Atlantic Deep Water (NADW) formation and around 60°S where surface waters are subducted to intermediate depth and then spread meridionally along isopycnals. Because of the larger interior ocean warming in the overshoot scenarios and long timescale of ocean mixing, it takes longer for the excess heat to be released. Faster warming of the sea surface relative to the interior and weaker AMOC contribute to ocean stratification that slows the reversal of ocean warming further. A larger temperature increase thus persists below the subsurface to a depth of about 2,000 m relative to RCP2.6 when the cumulative emissions overshoot is removed.

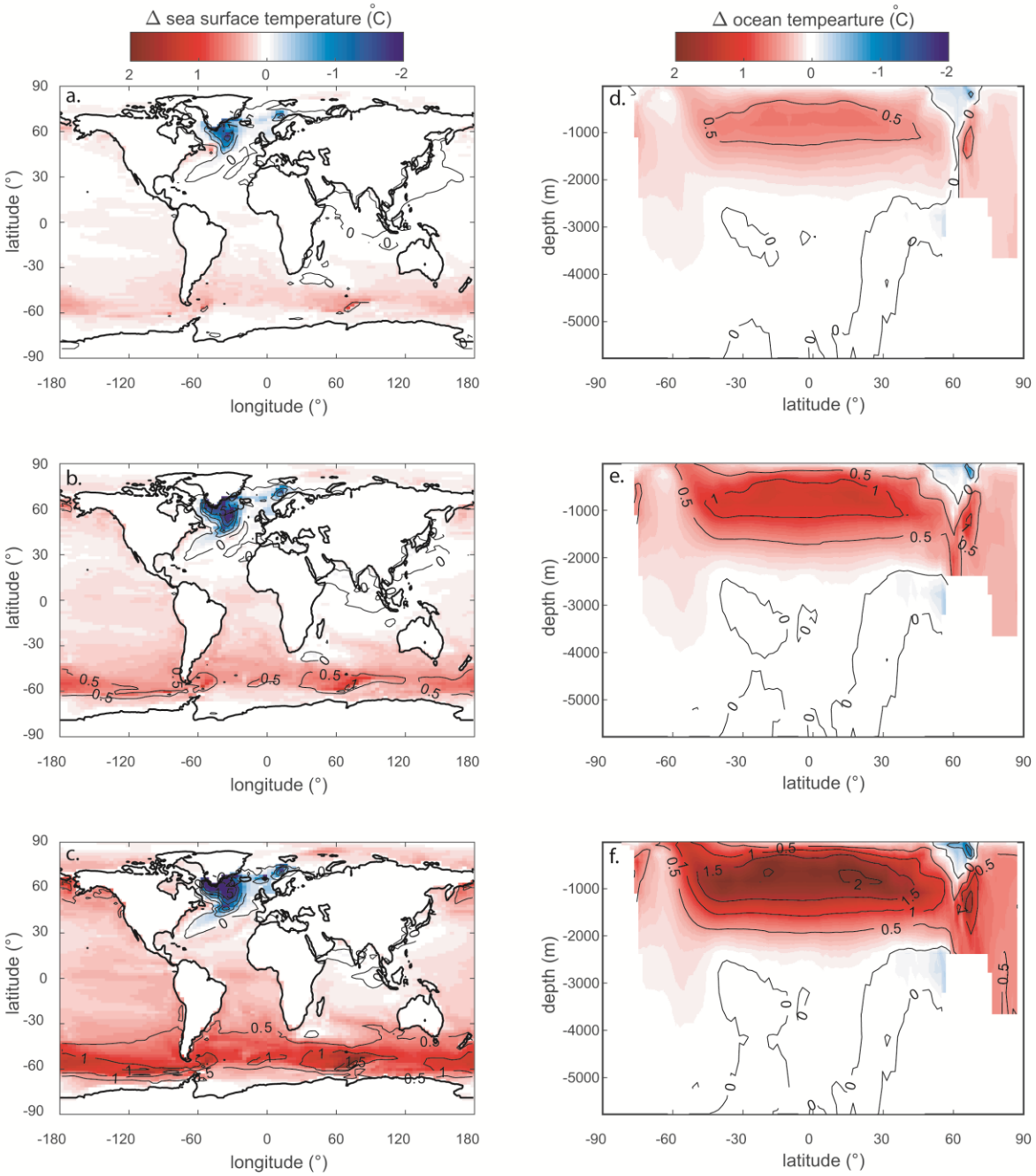

Figure 2. Spatial distribution of ocean temperature anomalies relative to the reference scenario RCP2.6 in 2300. **a-c,** latitude-longitude distribution of sea surface temperature anomaly (°C). **d-f,** zonal mean anomaly of ocean temperature (°C). **a&d**, RCP4.5-CDR5 minus RCP2.6. **b&e,** RCP6-CDR9 minus RCP2.6. **c&f,** RCP8.5-CDR15 minus RCP2.6.

In year 2300, large sea surface areas show a decrease in DO concentration relative to preindustrial except the North Atlantic south of Greenland and the polar regions in both hemispheres, which exhibit DO increase (Figure S9a-d). In the North Atlantic, the sea surface DO concentration in the overshoot scenarios is larger than in RCP2.6 in 2300 (Figure 3a-c), mainly driven by the lower SST in that region (Figure 2a-c). The DO concentration is also larger

in the Southern Ocean south of 60°S, particularly in the Weddell Sea (Figure 3a-c). The decline in sea ice area south of 60°S relative to preindustrial is larger in the overshoot scenarios than in RCP2.6 in 2300 (Figure S10). The larger sea ice decline could lead to stronger air-sea oxygen exchange and thus a higher DO concentration south of 60°S. The sea surface DO concentration decreases between 50°S and 60°S relative to RCP2.6 (Figure 3a-c), largely caused by the larger SST increase in this region (Figure 2a-c).

Changes in DO concentration relative to preindustrial are larger in the overshoot scenarios in vast parts of the interior ocean in 2300 (Figure S9e-h), with both negative and positive DO anomalies relative to RCP2.6 (Figure 3d-f). The DO concentration is larger than in RCP2.6 between 60°S and 60°N at 200-1,400 m depth (particularly in the latitudinal bands of 40°N to 60°N and 40°S to 60°S). The DO increase between 40°N and 60°N largely occurs in the North Pacific (Figure S11), where the meridional overturning circulation strengthens and ventilation is enhanced in the overshoot scenarios relative to RCP2.6 (Figure S12, S13). The enhanced overturning in the North Pacific has previously been shown to occur in response to weakened AMOC in the UVic ESCM (Saenko et al., 2004; Zickfeld et al., 2008). Changes in biological processes in the North Pacific are inconsistent with the positive DO anomaly at mid depth, suggesting that the dominant driver of this anomaly is increased ventilation. Net primary production increases in the eastern North Pacific leading to increased detrital export and remineralization (Figure S14-17), which are expected to cause a decrease in DO concentration and an increase in nutrient concentration at depth, both of which are opposite to the response simulated by the model (Figure3d-f, S17). The enhanced ventilation, on the other hand, transports more oxygen to depth and more nutrients into the surface layer, consistent with model response (Figure S18). The DO increase at intermediate depths between 40°S and 60°S is associated with the increased meridional overturning circulation in the Southern Ocean (Figure S19). The Southern Hemisphere westerlies strengthen relative to RCP2.6 in 2300 (Figure S7), leading to stronger subduction of surface waters and subsequent northward transport along isopycnals. This process transports oxygen from the sea surface to intermediate depths, thereby increasing the DO concentration of intermediate waters north of 60°S relative to RCP2.6 in 2300.

The DO concentration declines at 1,500-3,000 m depth around 60°N relative to RCP2.6 in 2300 (Figure 3d-f) due to a weaker AMOC (Figure S8b-e), which results in reduced ventilation of deep waters in regions where NADW is formed. The DO concentration also decreases at depth south of 60°S, potentially driven by the reduced Antarctic Bottom Water formation and inflow of NADW with reduced DO concentration that results from reduced deep-water formation in the North Atlantic relative to RCP2.6 in 2300 (Figure S8, 19). Enhanced remineralization of interior ocean detritus could also contribute to the DO decrease (Figure S15,16).

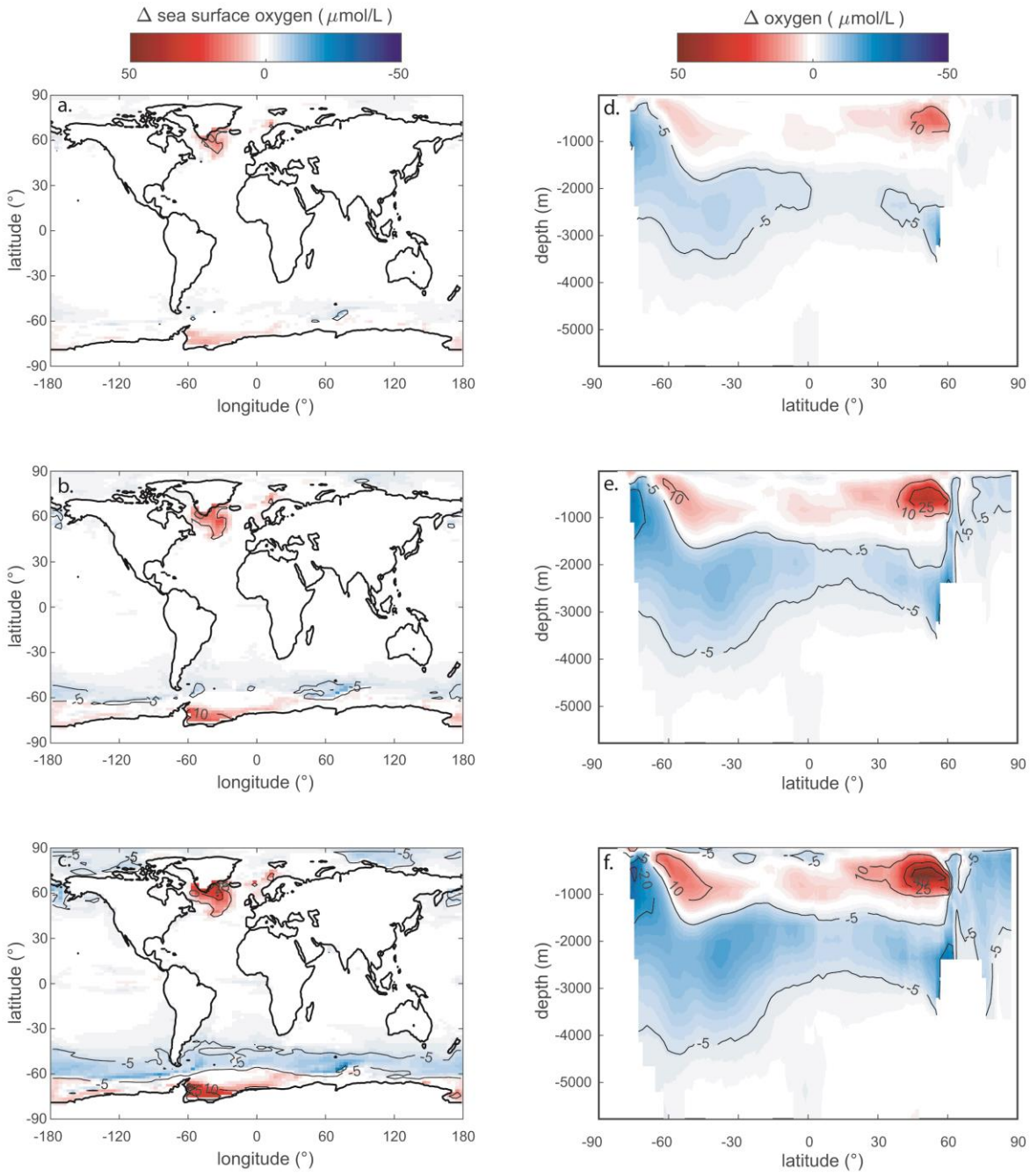

Figure 3. Spatial distribution of ocean dissolved oxygen (DO) concentration anomaly relative to the reference scenario RCP 2.6 in 2300. **a-c,** latitude-longitude distribution of sea surface DO concentration anomaly (μmol/L). **d-f,** zonal mean anomaly of ocean DO concentration (μmol/L). **a&d**, RCP4.5-CDR5 minus RCP2.6. **b&e,** RCP6-CDR9 minus RCP2.6. **c&f,** RCP8.5-CDR15 minus RCP2.6.

Ocean pH declines in large areas both at the sea surface and at depth relative to preindustrial in 2300, particularly in the Arctic (Figure S20). At the sea surface, the pH decrease in the overshoot scenarios is smaller than in RCP2.6 (consistent with the slightly lower atmospheric CO_2 concentration), except in the Arctic where a larger pH decrease is evident in the overshoot scenarios (Figure 4a-c). In the interior ocean, the pH decrease relative to RCP2.6 is

largely located at 300-2,000 m depth in the latitudinal band of 45°S to 45°N and in the Arctic in 2300 (Figure 4d-f).

Ocean pH declines with increasing carbon uptake by the ocean. Regional patterns of changes in ocean pH correspond to spatial patterns of changes in dissolved inorganic carbon (DIC) concentration (Figure 4d-f, S21). In 2300, DIC concentration remains higher in the overshoot scenarios than in RCP2.6 between 45°S and 45°N and in the Arctic (Figure S21, S22). The higher DIC concentration is associated with the slow upward mixing of excess carbon and enhanced stratification relative to RCP2.6, the same processes that delay the reversal of OT and DO changes. Lower pH in the Arctic relative to RCP2.6 in 2300 is attributed to the difference in sea ice area. During the period of rising surface air temperature, Arctic sea ice area declines more strongly in the overshoot scenarios than in RCP2.6 (Figure S23), allowing for larger CO_2 uptake. Arctic sea ice recovers after surface air temperature starts to decline, which hampers the release of CO_2 back to the atmosphere. Even though the sea ice area is smaller in the overshoot scenarios than in RCP2.6 in 2300 (Figure S24), the larger DIC anomaly persists.

The pH decrease lowers the aragonite saturation state, which influences the calcification rates of marine calcifying organisms. The aragonite saturation horizon shoals substantially relative to preindustrial, especially in the Arctic, due to soaring atmospheric CO_2 (Figure 4d-f). This shoaling is larger in the overshoot scenarios than in RCP2.6, with greater shoaling in scenarios with higher cumulative emissions overshoot. When the cumulative emissions overshoot is removed (year 2300), the aragonite saturation horizon in the overshoot scenarios is largely restored to the level in RCP2.6 except in the Arctic where it shoals to about 100 m (RCP8.5-CDR15) to 900 m (RCP4.5-CDR5) below the surface, compared to 1400 m in RCP2.6 (Figure 4d-f). The difference in shoaling of the aragonite saturation horizon results from the strong pH decrease relative to RCP2.6 in the Arctic in 2300.

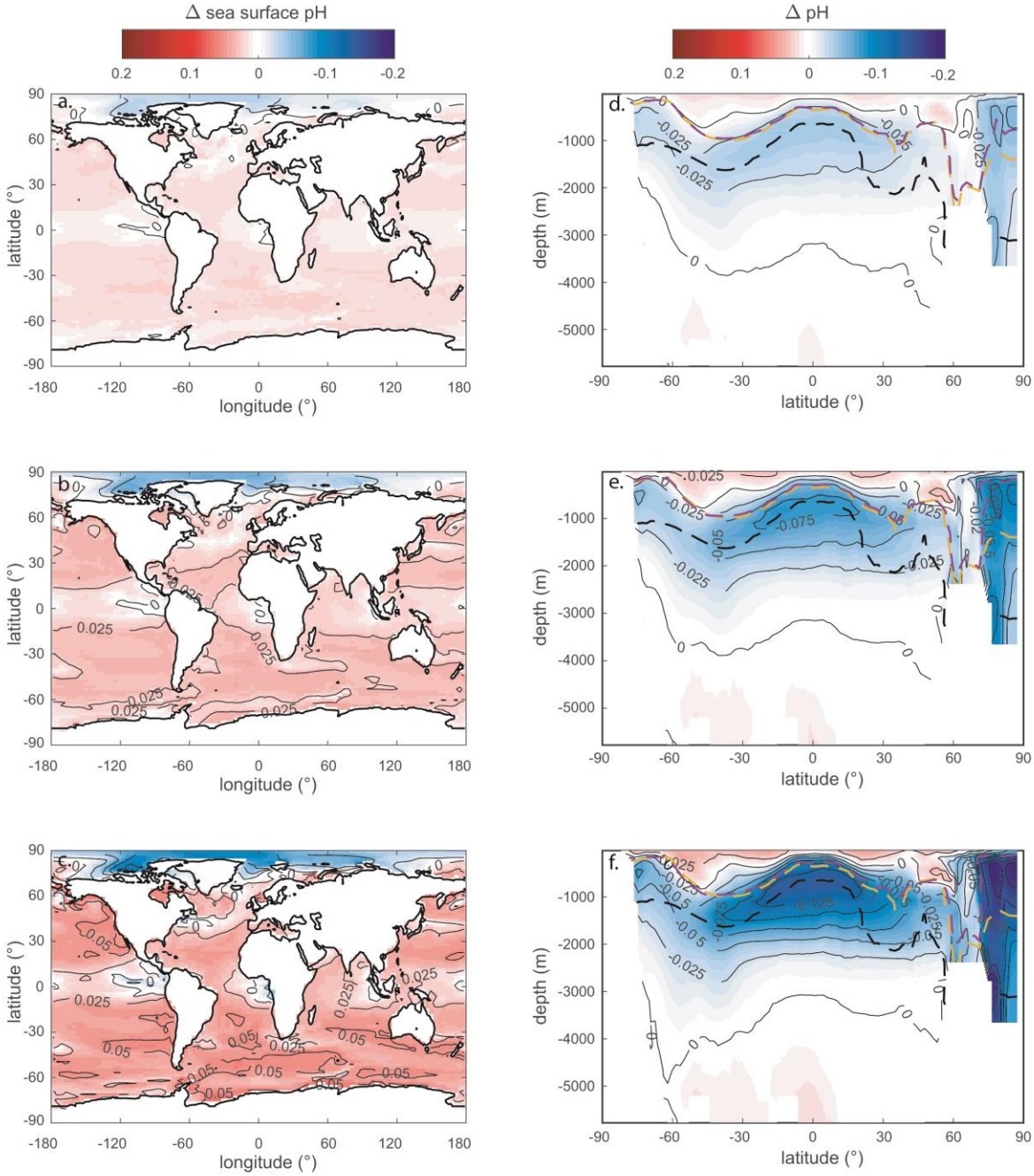

Figure 4. Spatial distribution of ocean pH anomaly relative to the reference scenario RCP2.6 in 2300. **a-c,** latitude-longitude distribution of sea surface pH anomaly. **d-f,** zonal mean anomaly of ocean pH. **a&d**, RCP4.5-CDR5 minus RCP2.6. **b&e,** RCP6-CDR9 minus RCP2.6. **c&f,** RCP8.5-CDR15 minus RCP2.6. The black and yellow dashed lines in panels d-f represent the aragonite saturation horizon under pre-industrial conditions and in RCP2.6 in 2300, respectively. The purple dashed lines represent the aragonite saturation horizon in the respective overshoot scenario.

4 Discussion and Conclusions

Our results suggest that net negative CO_2 emissions allow for a fast reversal of atmospheric CO_2 concentration, global mean surface air temperature and sea surface conditions in scenarios where a given cumulative CO_2 emissions and hence temperature limit is first exceeded. These global average results, however, hide substantial regional differences: for instance, SSTs are about 2°C warmer in the Antarctic Circumpolar Current, and more than 2°C colder in the North Atlantic in the scenario with the largest degree of overshoot relative to the reference scenario RCP2.6. Furthermore, large differences exist in average ocean values of temperature, dissolved oxygen concentration and pH, with larger differences for scenarios with higher levels of overshoot. There are also significant differences in the interior ocean distribution of these variables. In 2300, ocean temperature is up to 2°C warmer in the subsurface tropical ocean and pH up to 0.2 units lower in the Arctic relative to RCP2.6. These results suggest that negative CO_2 emissions are ineffective at reversing changes in the marine environment on human timescales (decades to a century), particularly following high levels of cumulative CO_2 emissions overshoot.

The fast reversal of atmospheric CO_2 and SAT are in agreement with previous studies exploring the Earth system response to negative CO_2 emissions (Cao & Caldeira, 2010; Tokarska & Zickfeld, 2015; Jones et al., 2016). The reversal of changes in sea surface variables on decadal timescales and in global ocean variables on multi-centennial timescales in response to net negative anthropogenic emissions are consistent with the findings of Mathesius et al. (2015) and can be expected to be robust across models, as they are in line with our understanding of the different timescales that govern uptake of heat and CO_2 by the ocean (Archer et al., 1997). The spatial distribution of the differences of ocean temperature, pH and DO concentration in RCP8.5-CDR15 relative to RCP2.6 is broadly in agreement with that shown in Mathesius et al. (2015), with regional differences due to different responses in ocean circulation. A salient feature of the UVic ESCM employed for this study is the onset of convection in the North Pacific following weakening of the meridional overturning circulation in the Atlantic. As Saenko et al. (2004) argues, this effect is physically plausible and is consistent with climate reconstructions.

The slow upward mixing of heat and gases (e.g. CO_2, O_2), weakened overturning circulation and increased stratification are important factors that hamper reversal of conditions in the ocean's interior to the state in RCP2.6. Due to the coarse resolution of the model employed in this study, diapycnal mixing and deep-water formation are heavily parameterized, leading to potential biases in the recovery timescale. Another possible source of bias is the lack of a dynamic land ice module in the UVic ESCM v2.9. The climate system response of melting land ice and continental ice sheets that produce freshwater input causing weakening of global overturning circulation is not included in our analysis. Previous studies suggest that land ice would continue to melt for centuries to millennia (Lemke et al., 2007), slowing the recovery of the overturning circulation. The overestimated AMOC recovery timescale possibly leads to overestimation of the degree of reversibility of changes in ocean conditions. The emission scenarios used in this study are idealized and may not be consistent with emissions from different gases. Radiative forcing from non-CO_2 greenhouse gases and aerosols follows RCP 2.6 in all scenarios, irrespective of the CO_2 emission rate in individual scenarios. As many gases are co-emitted with CO_2 (Rogelj et al., 2014), non-CO_2 forcing would likely be higher in the overshoot scenarios, implying larger ocean heat uptake during the overshoot phase and delayed recovery of the interior ocean temperature and DO concentration.

The larger changes in marine conditions in the overshoot scenarios relative to RCP2.6 in 2300 imply potentially detrimental effects on marine ecosystems. The warmer ocean could fundamentally affect biological processes, as most biological rates are temperature dependent (Eppley, 1972). Most marine species are sensitive to thermal stress (Gattuso et al., 2015). The increasing temperature in the Tropics could shift species distributions poleward, thereby reducing biodiversity in that region (Thomas et al., 2012). While DO increase in the tropical Indian Ocean and the Southern Pacific could alleviate hypoxia in these regions, the DO decrease in some coastal regions of the tropical Atlantic and Southern Ocean (Figure S11) could exacerbate hypoxia leading to mortality and habitat compression (Mislan et al., 2017). The reduced ocean pH leads to shoaling of the aragonite saturation horizon, particularly in the Arctic, which enhances the vulnerability of organisms that build shells or other structures of aragonite, such as deep-sea corals (Cao et al., 2014; AMAP Assessment, 2013).

We conclude that cumulative CO_2 emissions overshoot and subsequent return to a climate target state would leave a substantial legacy in the marine environment for centuries, particularly for scenarios with large levels of overshoot. Thus, our findings support the view that early CO_2 emissions involve lower risks for the marine environment than delayed emissions reduction followed by CDR (Seneviratne et al., 2018), as CDR cannot entirely restore the climate system to a state reached following a low emission scenario.

Acknowledgments

We would like to thank Margaret Valerio and Dr. Dana Ehlert for their helpful suggestions on the manuscript and for providing code for the analysis.

This research was funded by a Natural Sciences and Engineering Research Council of Canada (NSERC) Discovery Grant awarded to Dr. Kirsten Zickfeld (grant no. 402402-2011). Dr. Karen E. Kohfeld was supported by a Natural Sciences and Engineering Research Council Canada Research Chair Award.

The numerical simulations were performed using computing resources provided by Westgrid and Compute Canada. The model data used for the analysis will be deposited on Canada's Federated Research Data Repository (https://www.frdr.ca/repo/) upon acceptance of the manuscript for publication. The UVic ESCM version 2.9 code is available at http://climate.uvic.ca/model/2.9.

References

Arctic Monitoring and assessment programme (AMAP). (2013). AMAP assessment 2013: Arctic ocean acidification. Oslo, Norway. Viii + 99 pp., ISBN – 978-82-7971-082-0.

Archer, D., Kheshgi, H., & Maier-Reimer, E. (1997). Multiple timescales for neutralization of fossil fuel CO 2. Geophysical Research Letters, 24(4), 405–408. https://doi.org/10.1029/97GL00168

Bouttes, N., Gregory, J. M., & Lowe, J. A. (2013). The reversibility of sea level rise. *Journal of Climate*, *26*(8), 2502–2513. https://doi.org/10.1175/JCLI-D-12-00285.1

Cao, L., & Caldeira, K. (2010). Atmospheric carbon dioxide removal: Long-term consequences and commitment. *Environ. Res. Lett.*, *5*, 24011. Retrieved from http://dx.doi.org/10.1088/1748-9326/5/2/024011

Cao, L., Han, Z., Meidi, Z., & Shuangjing, W. (2014). Response of ocean acidification to a gradual increase and decrease of atmospheric CO2. *Environ. Res. Lett.*, *9*, 24012. Retrieved from http://dx.doi.org/10.1088/1748-9326/9/2/024012

Collins, M., Knutti, R., Arblaster, J., Dufresne, J.-L., Fichefet, T., Friedlingstein, P., & Al., E. (2013). Long-term Climate Change: Projections, Commitments and Irreversibility. *Climate Change 2013: The Physical Science Basis. Contribution of Working Group I to the Fifth Assessment Report of the Intergovernmental Panel on Climate Change*, 1029–1136.

Eby, M., Zickfeld, K., Montenegro, A., Archer, D., Meissner, K. J., & Weaver, A. J. (2009). Lifetime of anthropogenic climate change: Millennial time scales of potential CO2 and surface temperature perturbations. *Journal of Climate*, *22*(10), 2501–2511. https://doi.org/10.1175/2008JCLI2554.1

Eby, M. (2013). Historical and idealized climate model experiments: An intercomparison of Earth system models of intermediate complexity. *Clim. Past*, *9*, 1111–1140. Retrieved from http://dx.doi.org/10.5194/cp-9-1111-2013

Ehlert, D., & Zickfeld, K. (2017). What determines the warming commitment after cessation of CO 2 emissions? *Environmental Research Letters*, *12*(1), 015002. https://doi.org/10.1088/1748-9326/aa564a

Ehlert, D., & Zickfeld, K. (2018). Irreversible ocean thermal expansion under carbon dioxide removal. *Earth System Dynamics*, *9*(1), 197–210. https://doi.org/10.5194/esd-9-197-2018

Eppley. (1972). Temperature and phytoplankton growth in the sea. *Fish Bulletin*, *70*(4).

Frölicher, T., & Joos, F. (2010). Reversible and irreversible impacts of greenhouse gas emissions in multi-century projections with the NCAR global coupled carbon cycle-climate model. *Climate Dynamics*, *35*(7/8), 1439–1459. https://doi.org/10.1007/s00382-009-0727-0

Fyfe, J. C., Saenko, O. A., Zickfeld, K., Eby, M., & Weaver, A. J. (2007). The role of poleward-

intensifying winds on Southern Ocean warming. *Journal of Climate*, *20*(21), 5391–5400. https://doi.org/10.1175/2007JCLI1764.1

Gattuso, J.-P., Magnan, A., Billé, R., Cheung, W. W. L., Howes, E. L., Joos, F., et al. (2015). OCEANOGRAPHY. Contrasting futures for ocean and society from different anthropogenic CO_2 emissions scenarios. *Science (New York, N.Y.)*, *349*(6243), aac4722. https://doi.org/10.1126/science.aac4722

Gillett, N. P., Arora, V. K., Zickfeld, K., Marshall, S. J., & Merryfield, W. J. (2011). Ongoing climate change following a complete cessation of carbon dioxide emissions. *Nature Geoscience*, *4*(2), 83–87. https://doi.org/10.1038/ngeo1047

Jones, C. D., Ciais, P., Davis, S. J., Friedlingstein, P., Gasser, T., Peters, G. P., et al. (2016). Simulating the Earth system response to negative emissions. *Environmental Research Letters*, *11*(9), 095012. https://doi.org/10.1088/1748-9326/11/9/095012

Lemke, P., Ren, J., Alley, R. B., Allison, I., Carrasco, J., Flato, G., et al. (2007). Observations: Changes in snow, ice and frozen ground. *Climate Change 2007: The Physical Science Basis. Contribution of Working Group I to the Fourth Assessment Report of the Intergovernmental Panel on Climate Change*, 337–383. https://doi.org/10.1016/j.jmb.2004.10.032

Lowe, J. A., Huntingford, C., Raper, S. C. B., Jones, C. D., Liddicoat, S. K., & Gohar, L. K. (2009). How difficult is it to recover from dangerous levels of global warming? *Environmental Research Letters*, *4*(1). https://doi.org/10.1088/1748-9326/4/1/014012

MacDougall, A. H. (2013). Reversing climate warming by artificial atmospheric carbon-dioxide removal: Can a Holocene-like climate be restored? *Geophysical Research Letters*, *40*(20), 5480–5485. https://doi.org/10.1002/2013GL057467

Mathesius, S., Hofmann, M., Caldeira, K., & Schellnhuber, H. J. (2015). Long-term response of oceans to CO2 removal from the atmosphere. *Nature Climate Change*, *5*(12), 1107–1113. https://doi.org/10.1038/nclimate2729

Matthews, H. D., & Caldeira, K. (2008). Stabilizing climate requires near-zero emissions. *Geophysical Research Letters*, *35*(4), 1–5. https://doi.org/10.1029/2007GL032388

Meinshausen, M., Smith, S. J., Calvin, K., Daniel, J. S., Kainuma, M. L. T., Lamarque, J., et al. (2011). The RCP greenhouse gas concentrations and their extensions from 1765 to 2300. *Climatic Change*, *109*(1), 213–241. https://doi.org/10.1007/s10584-011-0156-z

Mislan, K. A. S., Deutsch, C. A., Brill, R. W., Dunne, J. P., & Sarmiento, J. L. (2017). Projections of climate-driven changes in tuna vertical habitat based on species-specific differences in blood oxygen affinity. *Global Change Biology*, *23*(10), 4019–4028. https://doi.org/10.1111/gcb.13799

Rogelj, J., Schaeffer, M., Meinshausen, M., Shindell, D. T., Hare, W., Klimont, Z., et al. (2014). Disentangling the effects of CO2 and short-lived climate forcer mitigation. *Proceedings of the National Academy of Sciences of the United States of America*, *111*(46), 16325–30.

https://doi.org/10.1073/pnas.1415631111

Rogelj, J., den Elzen, M., Höhne, N., Fransen, T., Fekete, H., Winkler, H., et al. (2016). Paris Agreement climate proposals need a boost to keep warming well below 2 °C. *Nature*, *534*(7609), 631–639. https://doi.org/10.1038/nature18307

Saenko, O. a, Schmittner, A., & Weaver, A. J. (2004). The Atlantic – Pacific Seesaw. *Journal of Climate*, *17*(11), 2033–2038. https://doi.org/10.1175/1520-0442(2004)017<2033:TAS>2.0.CO;2

Schmittner, A., Oschlies, A., Matthews, H. D., & Galbraith, E. D. (2008). Future changes in climate, ocean circulation, ecosystems, and biogeochemical cycling simulated for a business-as-usual CO2 emission scenario until year 4000 AD. *Global Biogeochemical Cycles*, *22*(1), 1–21. https://doi.org/10.1029/2007GB002953

Seneviratne, S. I., Phipps, S. J., Pitman, A. J., Hirsch, A. L., Davin, E. L., Donat, M. G., et al. (2018). Land radiative management as contributor to regional-scale climate adaptation and mitigation. *Nature Geoscience*, *11*(2), 88–96. https://doi.org/10.1038/s41561-017-0057-5

Solomon, S., Plattner, G.-K., Knutti, R., & Friedlingstein, P. (2009). Irreversible climate change due to carbon dioxide emissions. *Proceedings of the National Academy of Science, 106*, 1704–1709. https://doi.org/10.1073/pnas.0812721106

The National Academies Press. (2019). Negative Emissions Technologies and Reliable Sequestration. *Washington, D.C. National Academies Press.* Retrieved from https://www.nap.edu/catalog/25259

Thomas, M. K., Kremer, C. T., Klausmeier, C. A., & Litchman, E. (2012). A Global Pattern of Thermal Adaptation in Marine Phytoplankton. *Science*, *338*(6110), 1085 LP – 1088. Retrieved from http://science.sciencemag.org/content/338/6110/1085.abstract

Tokarska, K. B., & Zickfeld, K. (2015). The effectiveness of net negative carbon dioxide emissions in reversing anthropogenic climate change. *Environmental Research Letters*, *10*(9), 094013. https://doi.org/10.1088/1748-9326/10/9/094013

UNFCCC. (2015). Adoption of The Paris Agreement: Proposal by the President to the United Nations Framework Convention on Climate Change, *21932*(December), 1–32.

UNFCCC. (2016). The United Nations Framework Covention on Climate Change - Updated synthesis report on the aggregate effects of INDCs. Retrieved from http://unfccc.int/indc_portal/items/9240.php

UNFCCC. (1992). The United Nations Framework Convention on Climate Change. Article II. Retrieved from http://unfccc.int/essential_background/convention/background/items/1355.php

Weaver, A. J., Eby, M., Wiebe, E. C., Bitz, C. M., Duffy, P. B., Ewen, T. L. …Yoshimori, M. (2001). The UVic earth system climate model: Model description, climatology, and

adaptations to past, present and future climates. Atmosphere Ocean, 39(4), 361-428.

Zakhartsev, M., Johansen, T., Pörtner, H. O., Blust, R., Pörtner, H. O., Fernández, M., & Denny, M. W. (2004). Effects of temperature acclimation on lactate dehydrogenase of cod (Gadus morhua): genetic, kinetic and thermodynamic aspects. *Journal of Experimental Biology*, *207*(1), 95–112. https://doi.org/10.1242/jeb.00708

Zickfeld, K., Eby, M., & Weaver, A. J. (2008). Carbon-cycle feedbacks of changes in the Atlantic meridional overturning circulation under future atmospheric CO2. *Global Biogeochemical Cycles*, *22*(3), 1–14. https://doi.org/10.1029/2007GB003118

Zickfeld, K., Eby, M., Weaver, A. J., Alexander, K., Crespin, E., Edwards, N. R., et al. (2013). Long-Term climate change commitment and reversibility: An EMIC intercomparison. *Journal of Climate*, *26*(16), 5782–5809. https://doi.org/10.1175/JCLI-D-12-00584.1

Figure 1 in the manuscript.

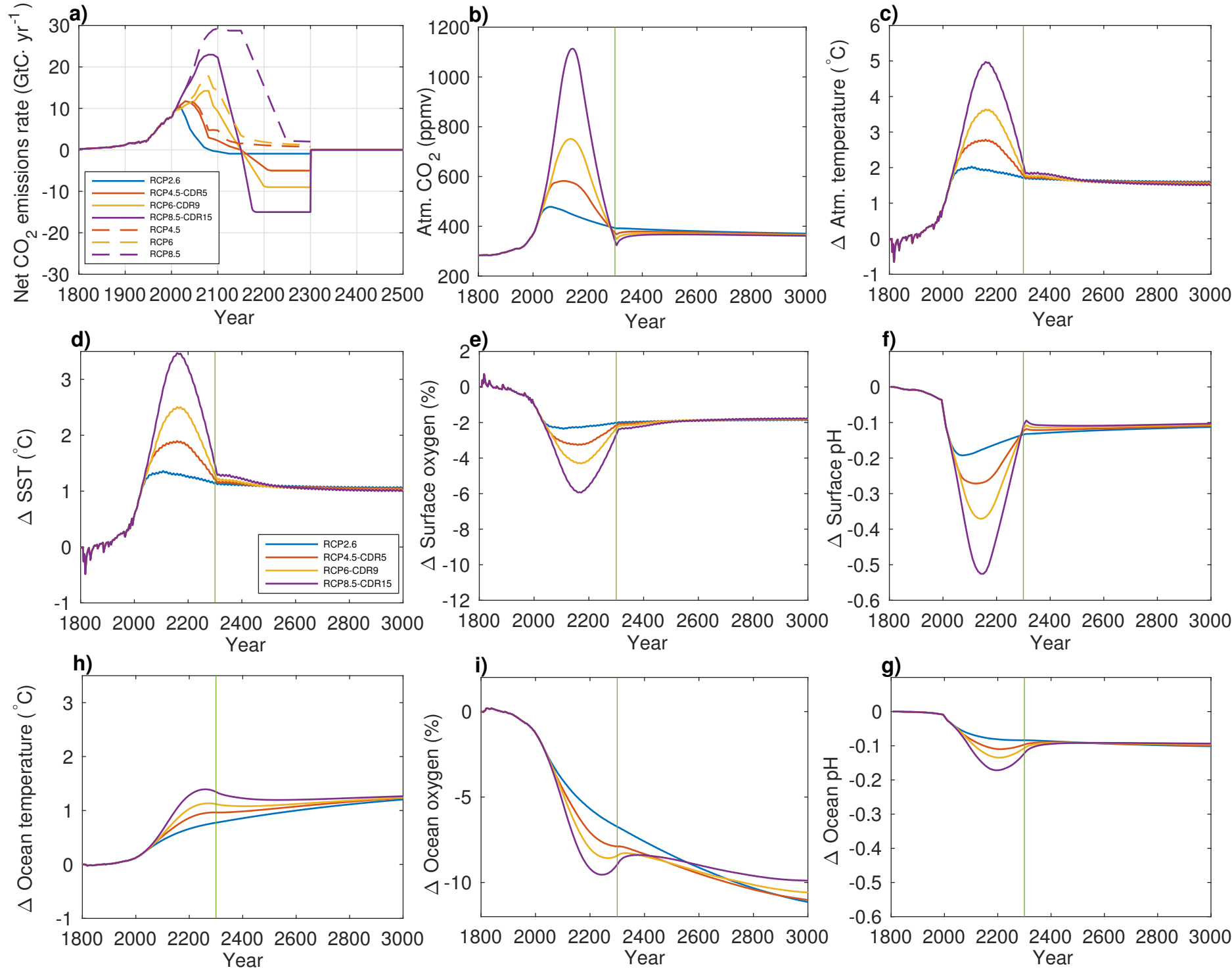
a)
b)
c)
d)
e)
f)
h)
i)
g)
Net CO_2 emissions rate (GtC· yr^{-1})
Atm. CO_2 (ppmv)
Δ Atm. temperature (°C)
Δ SST (°C)
Δ Surface oxygen (%)
Δ Surface pH
Δ Ocean temperature (°C)
Δ Ocean oxygen (%)
Δ Ocean pH
Year
RCP2.6
RCP4.5-CDR5
RCP6-CDR9
RCP8.5-CDR15
RCP4.5
RCP6
RCP8.5

Figure 2 in the manuscript.

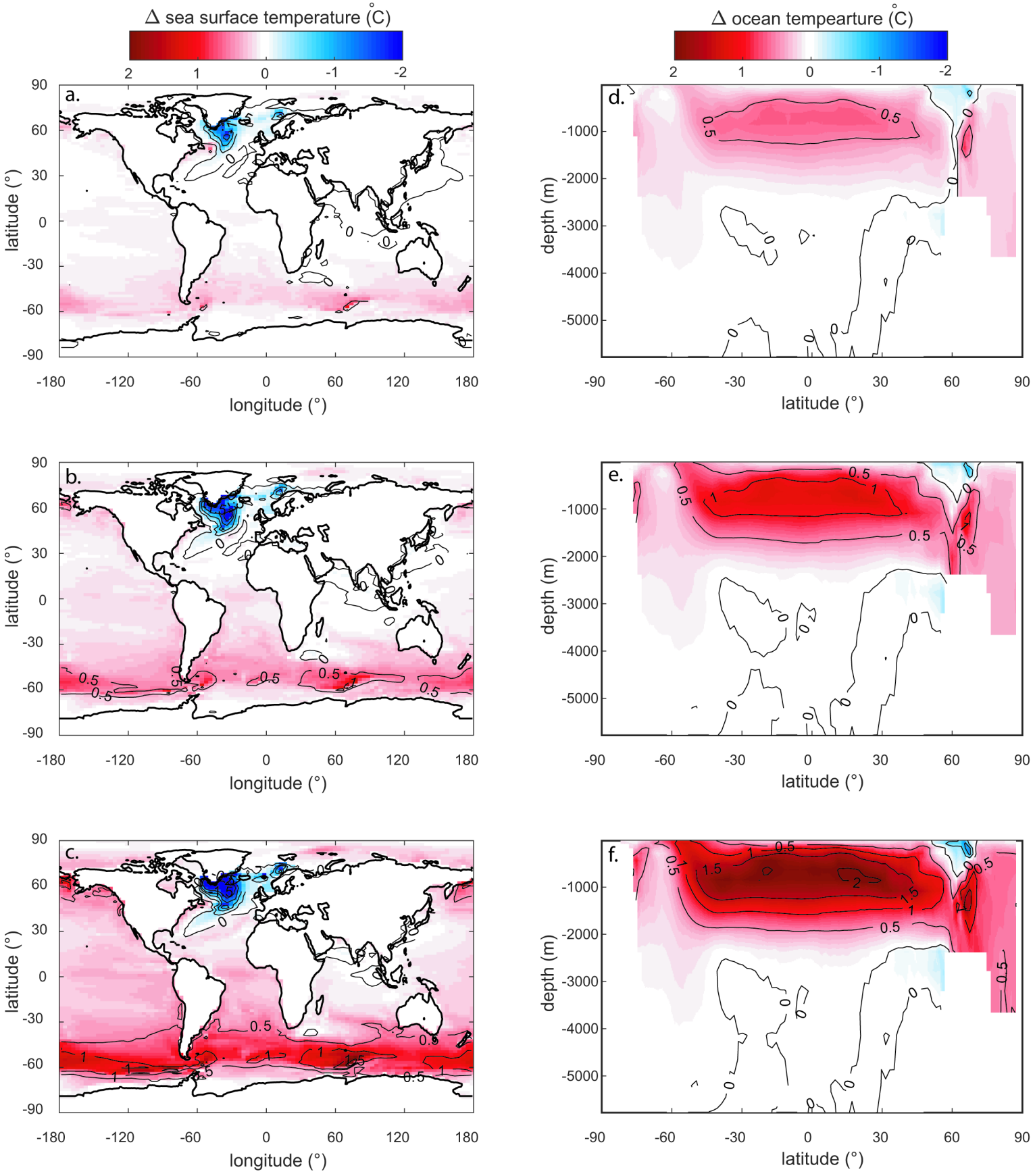
Δ sea surface temperature (°C)
2
1
0
-1
-2
a.
b.
c.
latitude (°)
longitude (°)
90
60
30
0
-30
-60
-90
-180
-120
-60
0
60
120
180
Δ ocean tempearture (°C)
d.
e.
f.
depth (m)
-1000
-2000
-3000
-4000
-5000
-90
-60
-30
0
30
60
90

Figure 3 in the manuscript.

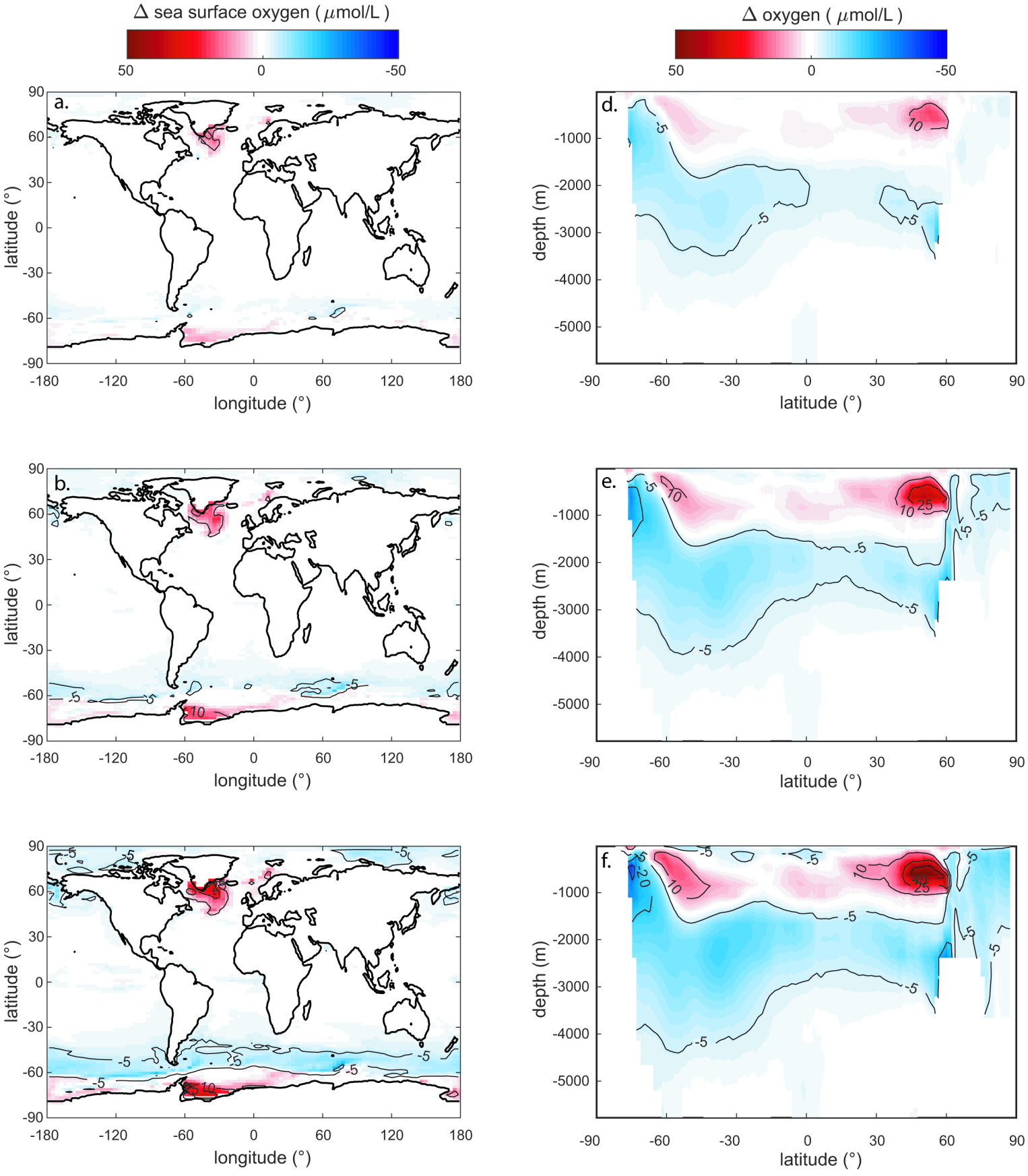
Δ sea surface oxygen (μmol/L)
50
0
-50
a.
latitude (°)
longitude (°)
b.
c.
Δ oxygen (μmol/L)
d.
depth (m)
latitude (°)
e.
f.

Figure 4 in the manuscript.

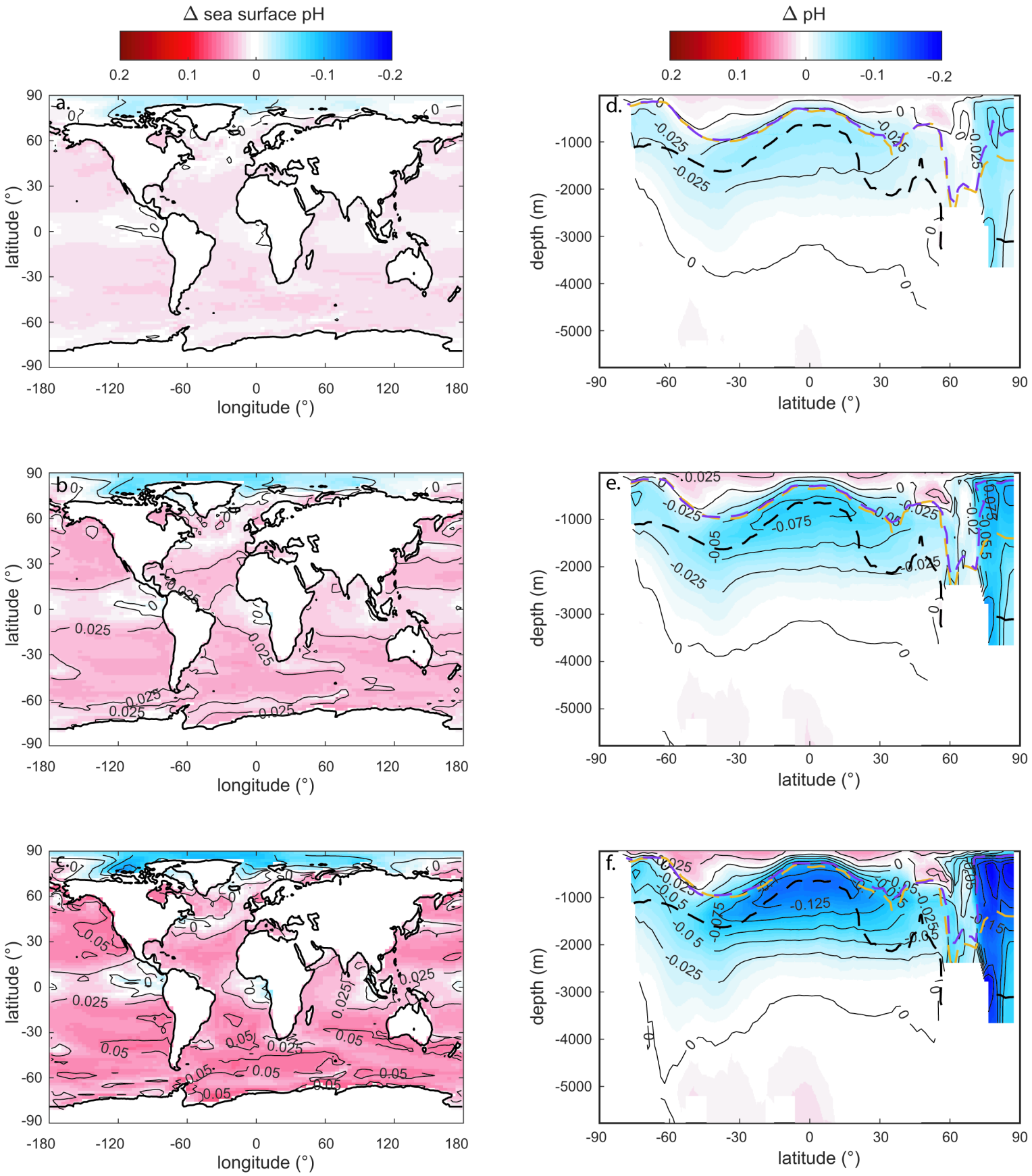
Δ sea surface pH
0.2
0.1
0
-0.1
-0.2
a.
b.
c.
latitude (°)
longitude (°)
Δ pH
d.
e.
f.
depth (m)
latitude (°)